In vivo hemin conditioning targets the vascular and immunological compartments and restrains prostate tumor development

Felipe M. Jaworski[1,2,3]; Lucas D. Gentilini[2,3]; Geraldine Gueron[1,3]; Roberto P. Meiss[4]; Emiliano G. Ortiz[1,3]; Paula M. Berguer[5]; Asif Ahmed[6]; Nora Navone[7]; Gabriel A. Rabinovich[8,9]; Daniel Compagno[2,3]; Diego J. Laderach[2,3,10,*] and Elba S. Vazquez[1,3,*]

[1] Universidad de Buenos Aires (UBA). Facultad de Ciencias Exactas y Naturales (FCEN). Departamento de Química Biológica (QB), Laboratorio de Inflamación y Cáncer. Buenos Aires, Argentina.

[2] Universidad de Buenos Aires (UBA). Facultad de Ciencias Exactas y Naturales (FCEN). Departamento de Química Biológica (QB), Laboratorio de Glico-Oncología Molecular y Funcional. Buenos Aires, Argentina.

[3] CONICET – Universidad de Buenos Aires (UBA). Instituto de Química Biológica de la Facultad de Ciencias Exactas y Naturales (IQUIBICEN). Buenos Aires, Argentina.

[4] Department of Pathology, Institute of Oncological Studies, National Academy of Medicine, Buenos Aires, Argentina.

[5] Fundación Instituto Leloir (FIL) – IIBBA – CONICET. Buenos Aires, Argentina.

[6] Aston Medical Research Institute, Aston Medical School, University of Aston, Birmingham, UK

[7] Department of Genitourinary Medical Oncology and the David H. Koch Center for Applied Research of Genitourinary Cancers, The University of Texas MD Anderson Cancer Center, Houston, TX 77030

[8] Laboratorio de Inmunopatología, Instituto de Biología y Medicina Experimental (IBYME), CONICET. Buenos Aires, Argentina.

[9] Universidad de Buenos Aires, Facultad de Ciencias Exactas y Naturales. Buenos Aires, Argentina.

[10] Departamento de Ciencias Básicas, Universidad Nacional de Luján, Argentina.

[*] Co-senior authors; to whom correspondence should be addressed.

Running title: Hemin conditioning restrains prostate tumor development.

Keywords: prostate-cancer; Heme-Oxygenase-1; conditioning; inflammation; Galectin-1.

Financial support: ANPCyT PICT RAICES 2013-0996 to ESV; ANPCyT PICT 2012-1533 to DC; ANPCyT PICT 2014-0983 to DJL

Corresponding authors: DJL and ESV; Intendente Guiraldes 2160, Piso 4, Pabellón II, Ciudad Universitaria (1428), Buenos Aires, Argentina; +5411-4576-3342; diegoladerach@qb.fcen.uba.ar; elba@qb.fcen.uba.ar

Word count: 4999 words

Total number of figures and tables: 4 figures and 2 tables (plus 2 supplementary tables and 3 supplementary figures).

Statement of translational relevance

Prostate cancer remains a major health care problem worldwide. Although most current therapies against this disease are designed to target the tumor cells themselves, the surrounding microenvironment plays a leading role in enabling the growth and dissemination of the tumor. Using a fully immunocompetent murine model, our results reveal how stromal conditioning with hemin, a well-known inducer of Heme Oxygenase-1 (HO-1), limits prostate cancer development by targeting both tumor vascularization and the cytotoxic T cell responses. Taken altogether, these data showcase a novel function of an already human-used drug as a means to boost the endogenous anti-tumor response.

Abstract

Purpose: Conditioning strategies constitute a relatively unexplored and exciting opportunity to shape tumor fate by targeting the tumor microenvironment. In this study we assessed how hemin, a pharmacological inducer of Heme Oxygenase-1 (HO-1), impacts upon prostate cancer (PCa) development in an in vivo conditioning model.

Experimental Design: The stroma of C57BL/6 mice was conditioned by subcutaneous administration of hemin prior to TRAMP-C1 tumor challenge. Complementary in vitro and in vivo assays were performed to evaluate hemin effect on both angiogenesis and the immune response. To gain clinical insight, we used PCa patient-derived samples in our studies to assess the expression of HO-1 and other relevant genes.

Results: Conditioning resulted in increased tumor latency and decreased initial growth rate. Histological analysis of tumors grown in conditioned mice revealed impaired vascularization. Hemin-treated HUVEC exhibited decreased tubulogenesis in vitro only in the presence of TRAMP-C1 conditioned media. Subcutaneous hemin conditioning hindered tumor-associated neo-vascularization in an in vivo Matrigel plug assay. Additionally, hemin boosted $CD8^+$ T-cell proliferation and degranulation in vitro and antigen-specific cytotoxicity in vivo. A significant systemic increase in $CD8^+$ T-cell frequency was observed in pre-conditioned tumor-bearing mice. Tumors from hemin-conditioned mice showed reduced expression of galectin-1 (Gal-1), key modulator of tumor angiogenesis and immunity, evidencing persistent remodeling of the microenvironment. We also found a subset of PCa patient-derived xenografts and PCa patient samples with mild HO-1 and low Gal-1 expression levels.

Conclusions: These results highlight a novel function of a human-used drug as a means of boosting the anti-tumor response.

Introduction

Prostate cancer (PCa) is the second most common cancer in men worldwide (1). Although most current therapies against this disease are designed to target the tumor cells, the surrounding microenvironment plays a leading role in enabling tumor development (2). Novel cancer therapies should consider the crosstalk between epithelial and stromal compartments, which has been reported to promote tumor progression by remodeling the extracellular matrix to enhance invasion and angiogenesis, releasing soluble factors and disarming the anti-tumor immune surveillance (3). Understanding the competing interactions between the several pro- and anti-tumorigenic components that shape the complex milieu of the tumor microenvironment, could lead to more integral approaches for cancer treatment (4).

Chronic inflammation has been associated with a high cancer incidence (5), providing clear evidence that a deregulated microenvironment affects tumorigenesis. An inflammatory setting fosters tumor progression through a wide range of mechanisms and represents a decisive factor in its evolution (6,7). Of note, inflammation-driven anatomical expansion and increased activation of the remodelled microvascular bed promotes angiogenesis and further influx of immune cells, which become co-dependent processes (8).

Several molecular pathways have been linked to cancer and inflammation (9). In particular, the enzyme Heme Oxygenase-1 (HO-1) is part of an endogenous defence system implicated in the homeostatic response (10,11). The intrinsic effect of HO-1 on tumor cells in different cancer models has been extensively addressed (12,13). Furthermore, data are available from a wide spectrum of physiopathological conditions that link HO-1 to modulation of angiogenesis and the immune function, two hallmarks of cancer (7).

In PCa, we have demonstrated that HO-1-over-expressing human xenografts generated in nude mice show impaired growth (14) and angiogenesis (15) and that this protein modifies the bone

microenvironment modulating PCa bone metastasis (16). We recently reported that HO-1 shapes cell-cell interactions, favoring a less aggressive phenotype (17,18). Moreover, HO-1 inhibited relevant pathways implicated in prostate tumorigenesis (16,19). Other groups have also provided evidence showing that HO-1 finely tunes PCa progression by exerting both pro-tumor (20, 21) and anti-tumor roles (22). However, in spite of considerable evidence regarding the role of this enzyme in the epithelial tumor cell compartment, its role in the tumour microenvironment still remains elusive.

Conditioning strategies constitute a relatively unexplored and exciting opportunity to shape tumor fate by targeting the tumor microenvironment. In this study we assessed whether conditioning with hemin, known to induce HO-1, affects PCa development using an immunocompetent murine model. Hemin treatment prior to tumor challenge resulted in a significant increase in tumor latency by targeting both tumor vascularization and cytotoxic T-cell responses. Taken altogether, these data showcase a novel function of an already human-used drug as a treatment to boost the endogenous anti-tumor response.

Materials and Methods

Cell culture. TRAMP-C1 cells (T-C1; ATCC) were cultured in DMEM (Invitrogen), 10% FBS (Gibco), Antibiotic-Antimycotic (Gibco) and insulin (5μg/ml). Cell morphology, androgen sensitivity and mycoplasma contamination were routinely assessed. Human umbilical vein endothelial cells (HUVEC; Lonza) were maintained in EGM-2 (Lonza). Bovine aortic endothelial cells (BAEC) were provided by MT Elola and cultured as previously described (23). Lymph node cell primary cultures were carried out in RPMI1640 (Invitrogen) containing 10% FBS (PAA), antibiotics, 2mM L-glutamine and 2×10^{-5}M β-mercaptoethanol. Hemin (Sigma-Aldrich) was dissolved in 1M Tris-HCl, pH 8; 0.5N NaOH; and PBS. This solution was 22μm-filtered and diluted in PBS or culture media.

Animals. Animal procedures complied with institutional guidelines. 6–8-wk-old male C57BL/6 mice were housed in the animal facility of the FCEN-UBA. *Foxn1*^{nu} mice were acquired from the animal facility of UNLP. T-cell receptor transgenic mice specific for H-2Kb $OVA_{257-264}$ (male OT-1 mice) were raised and tested at FIL-IIBBA-CONICET.

Hemin conditioning and subcutaneous tumor model. Mice were *s.c.* injected with hemin (200µl, 30µM) on days -8, -5 and -1 prior to challenge with 2×10^6 T-C1 cells on the same flank. Alternatively, hemin was administered on the contralateral flank when specified. Control littermates were injected with PBS. T-C1 cells were *s.c.* injected in Matrigel (4-5mg/ml; Corning). No changes in weight were detected. Euthanasia was practiced at the most when tumor volume reached 1500mm^3. Tumor size was calculated as $W^2\times L/2$ (W=width, L=length). Tumor volume was normalized to that at the start day of exponential growth.

Real-time reverse transcription-PCR. Transcriptional profile was analyzed in T-C1 tumor samples and lymph node samples, as previously described (23). Primers are listed in ***Table S1***. Human *PPIA*, murine *Rplp0*, and bovine *GAPDH* were used as internal reference genes.

Histological analysis. Sections obtained from paraffin-embedded tissues were stained according to Masson's trichrome technique or subjected to immunohistochemistry (IHC), as previously described (14,23), using anti-HO-1 (ab13243, abcam), anti-Gal-1 (H-45, Santa Cruz Biotechnology, Inc.), and anti-CD31 (D8V9E, Cell Signaling) antibodies. Blinded qualitative studies were carried out by a pathologist (RPM).

PCa patient-derived xenografts (PDXs) and tissue microarray (TMA) technology. PDXs were generated at MD Anderson Cancer Center (24) to prepare the TMA (n=50). IHC was carried out and

blinded semi-quantitative studies were performed (RPM): 0, no staining; 1, 2 and 3, low, mild, and high staining, respectively. Scores of individual blokes corresponding to the same PDX were averaged.

Tubulogenesis assay. 80%-confluent T-C1 cells were cultured for 24h in a 1:5 diluted growth media. Conditioned-media (CM) was harvested and filtered. 60µl of growth factor–reduced Matrigel was plated in a 96-well plate and incubated at 37°C for 15min. 12.5×10^3 hemin-treated (50µM, 8h) or control HUVEC were plated on the Matrigel in the presence of control or T-C1-derived CM. Positive control wells were seeded in EGM-2 medium. Endothelial tube formation was evaluated after 18h. Five fields per well were photographed. AdobePhotoshop-processed photographs were evaluated using the NIH ImageJ Angiogenesis Analyzer Plug-in.

Apoptosis assay. BAEC were treated with hemin (50µM, 8h), washed and subsequently cultured for 16h in a 1:5 diluted growth media containing recombinant Gal-1 (25) (0; 2.25; 4.5; and 9µM). Detached and adherent cells were photographed, harvested (TripLE Express, ThermoFisher) and stained with FITC-Annexin-V (Apoptosis Detection kit, BD Pharmingen) and propidium iodine (Sigma), followed by flow cytometry.

Wound healing assay. HUVEC were treated with hemin (50µM, 8h), washed and subsequently cultured for 24h in a 1:5 diluted growth media. CM was harvested and filtered. Confluent T-C1 cells were washed and serum-starved for 8h. A 1-mm wide scratch was made across the cell layer and, after washing with serum-free medium twice, hemin-treated or control HUVEC CM was added, and plates were photographed immediately and after incubation (12, 24, 48h) at the identical location of initial image. Wound area was quantified using NIH ImageJ.

Tumor-to-endothelium adhesion assay. 80% confluent HUVEC were treated with hemin (50µM, 8h) and subsequently washed. 3×10^4 CFSE-labeled T-C1 cells (2.5µM, 5min, 1×10^6 cells/ml in PBS 1%

FBS; Sigma) were added. After incubating 2h at 37°C, unattached cells were washed away and three different fields of each well were photographed. Cells were counted using the NIH ImageJ Cell Counter Plug-in.

***In vivo* Matrigel plug assay.** 2×10^6 T-C1 cells in 500µl of Matrigel (4-5mg/ml) were subcutaneously injected into mice following hemin conditioning. Five days later, Matrigel plugs were harvested and photographed. Plugs were homogenized in H_2O and cleared by centrifugation. Hemoglobin and total protein content were determined using the Drabkin's reagent (WienerLab) and the Pierce BCA Protein Assay kit (ThermoScientific).

Lymphocyte proliferation and degranulation assays. For T-cell proliferation assays, 5×10^5 CFSE-stained murine lymph node cells (2.5µM, 5min) were seeded in a 96-well U-bottomed plate. Hemin was added into culture (18.75, 37.5 and 75µM). 1×10^4 mitomycin-arrested T-C1 cells (3-hour treatment, 10µg/ml; Sigma) were added into cultures to mimic a tumor microenvironment. For T-cell degranulation, cells were stimulated with coated anti-CD3 antibody (145-2C11 hybridoma) (1µg/ml, 12h) and anti-CD107a was added (1h, 37°C; 1D4B, BD Pharmingen) followed by an additional 4h-culture with monensin (3µM; BD Pharmingen). Spontaneous expression of CD107a was also evaluated. For T-cell proliferation, cells were stimulated with coated anti-CD3 antibody (1µg/ml, 72h) and proliferation assessed by CFSE dilution. Cells were stained for CD8 (53-6.7, BD Pharmingen) in staining buffer (PBS 1% FBS, 0.01% sodium azide; 30min on ice). HO-1 induction was confirmed by intracytoplasmatic staining (ab13248; abcam). FACS was performed in a FACSAria (BD Biosciences) using the FlowJo software.

***In vivo* CTL assay.** WT C57BL/6 mice were irradiated (1Gy; ^{137}cesium source; Cebirsa), transferred with 3×10^6 OT-1 lymph node cells, and subcutaneously injected with hemin on a daily basis for 3 days. On the next day, freshly isolated WT C57BL/6 spleen cells were obtained by mechanical disruption and

erythrocytes were lysed. Splenocytes were stained with CFSE (5μM or 0.5μM). $CFSE_{dim}$ cells were incubated with OVA-derived SIINFEKL peptide (10μg/ml, 30 min, 37°C; Invivogen); $CFSE_{bright}$ cells were exposed to the vehicle alone. Mice were transferred with a 1:1 mix of $CFSE_{dim\text{-}OVA}$ and $CFSE_{bright\text{-}ctrl}$ cells (2×10^6 cells, 100μl). After 16h, spleens were processed for FACS analysis. Alternatively, hemin treatment was carried out *ex vivo* (75μM, 8h) prior to adoptive transfer. Mice with no previous transfer of OT-1 lymph node cells were used as a control to calculate specific cytotoxicity as follows: $SC=[1-(\%CFSE_{dim\text{-}OVA}/\%CFSE_{bright\text{-}ctrl})_{transferred\ mice}\times(\%CFSE_{bright\text{-}ctrl}/\%CFSE_{dim\text{-}OVA})_{non\text{-}transferred\ mice}]\times100$.

Flow cytometric analysis of murine samples. Tumor, spleen, tumor-draining lymph node (TDLNs; axillary, brachial and inguinal), and blood vessel-containing tissue samples were harvested and single-cell suspensions were obtained by mechanical disruption. Tumor samples were previously disaggregated with Collagenase type IV (1mg/ml, 1h, 37°C; Sigma). Cells were stained and analyzed by FACS. Anti-CD3-FITC (17A2; BD Biosciences), anti-CD11b-PE (M 1/70; BD Biosciences), anti-Gr-1-FITC (RB6-8CS; BD Biosciences), anti-CD31 (390, BD Pharmingen), anti-HO-1, goat-anti-rat Ig-PE (550767, BD Biosciences) goat-anti-mouse IgG1-Alexa488 (A21121, ThermoFisher Scientific) were used.

Bioinformatics analysis. We searched Oncomine (26) to identify human expression microarray datasets that compare prostate adenocarcinoma versus normal gland. ***Table S2*** shows information about these datasets. Cited literature was reviewed to confirm that the analysis was as documented.

Statistical analysis. At least three biological replicates (i.e. independent experiments) were carried out. Data represent mean ± SD. GraphPad software was used. Two groups were compared with the Student *t* test for unpaired data. Two-way ANOVA tests were used for multiple comparisons (with Tukey's and Bonferroni *post hoc* tests). Non-parametric Mantel-Cox tests were carried out when comparing tumor-free mice curves. $P<0.05$ was considered statistically significant.

Results

Hemin conditioning impairs PCa development

Given the scarce PCa pre-clinical models available allowing assessment of the whole tumor microenvironment, we used a syngeneic model based on the subcutaneous injection of T-C1 cells into C57BL/6 mice, previously standardized in our laboratory (27). TRAMP cells constitute the only murine PCa cells lines appropriate for implantation into syngeneic immunocompetent mice. To study whether hemin conditioning influences tumor development, mice (n=5) were subcutaneously injected with this agent (200µl; 30µM) on days -8, -5 and -1 prior to tumor challenge on the same flank ($2x10^6$ T-C1 cells in Matrigel) (***Figure 1A***). Control littermates (n=5) were injected with saline. Hemin dosage was not arbitrary chosen; it was adapted from the dose used for human porphyria. Pharmacokinetics, pharmacodynamics and toxicological studies have been performed in animals prior to hemin acceptance for use in humans. Although tumors developed in all the mice, pre-treatment resulted in a marked increase in tumor latency (57±3 days in hemin-treated mice vs. 47±5 days in control mice; ***Figure 1B****, left panel*). Furthermore, initial growth rate was significantly reduced in hemin-treated animals (***Figure 1B****, right panel*). Tumor histological analysis at the time of euthanasia showed lower number of blood vessels in the experimental group, as revealed by both trichrome staining and CD31 IHC (***Figure 1C***). Evaluation of mediators typically involved in angiogenesis (VEGF-A, CD142, uPA, FGFb, TIMP-1, TSP-1 and galectin-1 (Gal-1)) revealed that only the Gal-1-coding mRNA (*Lgals1*) expression was significantly reduced in hemin-treated animals (***Figure 1D***). Remarkably, our group and others have previously reported an up-regulated expression of this lectin in human PCa and its correlation with the tumor angiogenic phenotype (23, 28).

Hemin conditioning reprograms the angiogenic switch in PCa

Considering our previous findings that HO-1 and Gal-1 expression play a critical role in PCa neovascularization (15,23), we analyzed the effect of hemin on endothelial cells within a prostate tumor setting. HO-1 induction was confirmed by RT-qPCR (*Hmox1* mRNA; ***Figure 2A***). An *in vitro* tube

formation assay was performed using hemin pre-treated HUVEC, seeded onto Matrigel-coated wells in the presence or absence of T-C1-derived CM. Hemin pre-treatment dramatically inhibited tubulogenesis only in the presence of tumor CM (***Figure 2B***, ***Figure S1A***), as reflected by a significant reduction of total tube length (**Figure *2C***) and the number of master segments and tube joints in this experimental condition (***Figure S1B***). Importantly, the tube network was not hindered both in complete growth media and in the absence of T-C1-derived CM, confirming HUVEC viability is not significantly affected by hemin pre-treatment. To evaluate the role of Gal-1, we carried out an apoptosis assay in the presence of the recombinant lectin. Whilst control cells did not show Gal-1-induced apoptosis, hemin-treated endothelial cells were significantly more susceptible to cell death in a Gal-1 dose-dependent fashion (***Figure 2D***). Of note, hemin-treated cells did not show any significant differences in terms of basal cell death when compared to control cells. The increase in endothelial cell death was further supported by a significant decrease in CD146 mRNA levels (***Figure S2***), a co-receptor for VEGFR-2 and a decoy receptor for Gal-1 (29,30). We next studied whether hemin conditioning influences the crosstalk between tumor and endothelial cells. T-C1 cell motility was significantly impaired when a wound-healing assay was performed in the presence of hemin pre-treated HUVEC CM (**Figure *2E***). Tumor cell adhesion to endothelial cells was severely reduced when HUVEC were pre-treated with hemin (***Figure 2F***). We ruled out there were hemin traces in the CM by assessing *HMOX1* mRNA expression levels in T-C1 that had been exposed, and detected no significant differences (data not shown). Collectively, these findings suggest that hemin conditioning remodels the endothelial compartment and negatively regulates interactions between endothelial and tumor cells. To assess whether hemin pre-treatment is implicated in tumor neovascularization *in vivo*, we performed a Matrigel plug assay. C57BL/6 mice (n=5) were subjected to our hemin conditioning protocol before being injected with T-C1 cells in Matrigel. Control mice (n=5) were injected with saline-containing Matrigel. After 5 days, plugs were harvested and hemoglobin content was determined. In keeping with our *in vitro* findings, hemin pre-treatment significantly inhibited vascularization *in vivo* (***Figure 2G***). In summary, hemin conditioning impacts upon the angiogenic process, probably accounting for tumor

growth inhibition (***Figure 1B***). To verify that hemin conditioning induces HO-1 expression in endothelial cells, on the day that mice would have been challenged with tumor cells we collected samples of blood vessel-containing tissue from the same animal flank that had been previously injected with either PBS (n=5) or hemin (n=6). We subsequently assessed HO-1 expression in endothelial cells using FACS and we confirmed that hemin treatment *in vivo* results in increased HO-1 expression in $CD31^+$ cells (***Figure 2H***).

Hemin conditioning fosters $CD8^+$ T-cell responses

Both HO-1 and Gal-1 have been reported to play major roles in shaping anti-tumor responses (31,32). We thus analyzed hemin effect upon the immune compartment by performing *in vitro* co-cultures of lymph node cells isolated from C57BL/6 mice with syngeneic T-C1 cells. Hemin induced HO-1 in a dose-dependent fashion in $CD8^+$ cytotoxic T lymphocytes (CTLs), as determined by intracellular staining and flow cytometry (***Figure 3A***). FACS analysis of cell division by CFSE staining demonstrated that hemin increases $CD8^+$ T-cell proliferation in a dose-dependent manner in response to polyclonal activation (***Figure 3B***, left panel), even when co-cultured with tumor cells (***Figure 3B***, right panel). We also examined hemin effects on the cytotoxic potential of $CD8^+$ T-cells, by measuring the expression of CD107a on the cell surface as a result of CTL degranulation. Hemin treatment resulted in enhanced CTL effector function both in normal and tumor microenvironments (***Figure 3C***). To evaluate whether hemin also boosts the immune function in an established tumor immunosuppressive setting, lymph node cells and T-C1 cells were co-cultured 24h prior to hemin addition. Hemin augmented $CD8^+$ T-cell proliferation and degranulation even under these experimental conditions (***Figures 3D-E***), reverting tumor immunosuppression. To verify the relevance of these findings *in vivo*, we tested cytotoxicity following hemin conditioning by performing a CTL assay. $CD8^+$ T cell effector function *in vivo* was determined by mixed transfer of OVA peptide-pulsed target cells with control cells into WT C57BL/6 mice previously transferred with OT-1-derived lymph node cells (n=5) (***Figure 3F***). We confirmed that hemin treatment induced HO-1 expression at the transcriptional level in lymph node samples collected

on the day that mice would have been transferred with the mix (***Figure 3G***). The left panel of ***Figure 3H*** shows representative results, where the relative frequencies between peptide-pulsed target cells and control cells were used as readouts of specific killing. The frequency of $CFSE_{dim\text{-}OVA}$ cells was reduced to a greater extent in hemin-treated mice compared to control littermates. OVA-specific cytotoxicity was significantly enhanced when transferred mice were subcutaneously treated with hemin prior to challenge with OVA-loaded cells (***Figure 3H***, right panel). We next sought to determine whether hemin boosts antigen-specific cytotoxicity *in vivo* if OT-1 lymph node cells were treated *ex vivo* prior to adoptive transfer into WT C57BL/6 mice. Hemin-treated lymphocytes led to augmented OVA-specific cytotoxicity (***Figure 3I***). Our results indicate that the sole exposure of lymph node cells to hemin boosts $CD8^+$-mediated cytotoxicity, which could account for tumor growth inhibition (***Figure 1B***).

Hemin conditioning targets the vascular and immunological compartments and restrains prostate tumor development

To investigate whether hemin conditioning influences vascular and immunological compartments at earlier stages of tumor development, tumor-bearing C57BL/6 mice (n=4) were sacrificed when control mice exhibited tumors in their exponential growth phase while hemin pre-treated mice showed tumors in their initial growth steps. The frequency of $CD3^+CD8^+$ cells in hemin-conditioned mice was systemically increased, as determined by immunophenotyping the tumor, draining lymph nodes and spleen (***Figure 4A***). Furthermore, the frequency of regulatory $Gr\text{-}1^+CD11b^+$ myeloid cells in the tumor-draining lymph nodes was reduced in hemin pre-treated mice compared to control animals (***Figure 4B***), probably allowing a more effective anti-tumor immune response. Histological analysis revealed that control tumors, but not tumors derived from hemin-conditioned mice, showed dilated blood vessels mimicking an angiomatous image (***Figure 4C***, upper and central panels). Additionally, hemin pre-treated animals displayed tumors with reduced atypical mitotic figures when compared to control mice (***Figure 4C***, lower panel). IHC revealed lower levels of Gal-1 expression in tumors generated under hemin conditioning (***Figure 4D***). These results further emphasize the essential role of the tumor

microenvironment in governing the fate of tumor development. Considering the systemic changes in conditioned mice (***Figures 4A-B)***, we next evaluated whether hemin exerts an anti-tumor effect when injected at a site other than the flank subsequently challenged with the tumor cells. Similar to hemin conditioning on the ipsilateral flank, its administration on the contralateral flank also led to a significant increase in tumor latency (45±5 days in control mice, n=8; 56±3 days in ipsilateral conditioned animals, n=10; and 55±2 days in the contralateral-conditioned group, n=5; ***Figure 4E***). No significant differences were found between both conditioning strategies in terms of tumor latency, suggesting both treatments had a similar anti-tumor effect. Furthermore, in an effort to elucidate the relative contribution of the vascular and immune compartments, we tested if hemin conditioning was able to modulate tumor development in athymic nude mice. Tumor latency and growth did not significantly differ when comparing hemin-conditioned animals with control mice (***Figure 4F***), confirming that the immune system is required to target PCa tumors in our experimental model.

Bioinformatic analysis of human prostate adenocarcinoma microarray datasets

To address potential clinical implications of elevated HO-1 expression in human prostate tumor samples, we searched the microarray database Oncomine (26). We found 16 gene expression microarray datasets comparing prostate adenocarcinoma versus normal prostate tissue that met our eligibility criteria (***Table S2***). Only 4 datasets presented increased expression for *HMOX1* mRNA with $P<0.05$ (***Table 1***), in which only one of these datasets showed fold induction greater than 1.5. These results support the idea that HO-1 expression is not associated to prostate carcinogenesis. Given the small *P*-values obtained for these 4 datasets (n=122, n=112, n=150, n=19; refer to ***Table S2***), we extended our analysis to assess the expression levels for *LGALS1*. ***Table 1*** sums up the results obtained with all the datasets, whereas ***Figure S3*** depicts representative results obtained when assessing Grasso Prostate Statistics (33). Interestingly, the expression profile for *LGALS1* showed significant down-regulation for prostate adenocarcinoma vs. normal gland in samples where *HMOX1* was up-regulated (***Table 1*** *and* ***Figure S3***). We assessed in these same datasets the expression

profiles of different angiogenesis-related genes (*CD34*, *FLT1*, *FLT4, KDR, VEGFA* and *VEGFC*). Accordingly, their expression levels were down-regulated for the prostate adenocarcinoma vs. normal gland comparisons in which *HMOX1* was up-regulated (***Table 1*** *and* ***Figure S3***). On the contrary, these datasets with increased expression of *HMOX1* also exhibited *VCAM1, CD28, CD80* and *CD86* up-regulation in prostate adenocarcinoma compared with the normal gland (***Table 1*** *and* ***Figure S3***). Interestingly, more intense lymphocyte infiltration was observed in tumors with elevated VCAM-1 (34). Furthermore, *CD28, CD80* and *CD86* constitute key co-stimulatory molecules required to mount an effective immune response, and their elevated expression levels are indicative of T-cell activation. These results support the aforementioned findings and point towards a subset of patients who might respond to anti-angiogenic and/or immune stimulatory therapy.

Histological analysis of HO-1 and Gal-1 in human PCa patient-derived xenografts

To further understand potential clinical implications, we screened a TMA containing 50 PDXs, each represented by PDXs grown in three different mice and three cores per tumor. These xenografts were derived from primary prostate cancer and metastatic sites, and encompass samples of advanced prostate cancer with various histopathological patterns. PDXs with heterogeneous staining between different cores or tumors for either HO-1 or Gal-1 were excluded from the analysis. PDXs were classified according to HO-1 immunostaining and we studied in detail those with low-to-intermediate HO-1 staining. This subset of PDXs displayed two clear clusters with either low or high Gal-1 immunostaining (***Table 2***). Those PDXs with mild HO-1 and low Gal-1 expression could be potentially more susceptible to an anti-angiogenic and/or immune therapy, and could even benefit from the anti-angiogenic properties of HO-1 induction (15).

Discussion

Carcinogenesis is a multi-step process encompassing mechanisms in both the epithelial cell and the surrounding tissue. Numerous signaling pathways are involved in the dynamic crosstalk between these compartments, and their deregulation influences disease initiation, progression and patient prognosis (2). Novel experimental strategies have been designed to re-educate the microenvironment in order to shift the balance towards an anti-tumorigenic profile (4). Here we designed an experimental protocol using a murine model to shape the niche where prostate tumor cells are subsequently implanted (***Figure 1***). We demonstrate for the first time that hemin conditioning remodels the bidirectional interactions between the tumor and the surrounding tissue, affects tumor neo-vascularization and immune function and impairs tumor growth. Our results indicate that hemin conditioning acts, at least in part, through the inhibition of angiogenesis and the potentiation of tumor immunity, thus restraining PCa development. Our findings also demonstrate that hemin modulated tumor development when injected on the contralateral flank (***Figure 4E***). This strategy led to an increase in tumor latency that was comparable to that corresponding to ipsilateral hemin conditioning, further supporting potential novel therapeutic avenues for PCa. Of note, hemin is approved for use in treatments against acute intermittent porphyria.

Angiogenesis is essential for tumor development given that proliferation of cancer cells, as well as their metastatic spread rely on an adequate supply of both oxygen and nutrients and the removal of waste products. We demonstrate that hemin conditioning inhibits tumor-associated neo-vascularization *in vitro* and *in vivo* (***Figures 2 and 4***). Hemin pre-treatment of HUVEC dramatically hindered tubulogenesis only in the presence of tumor CM, suggesting hemin-treated HUVEC are refractory to pro-angiogenic tumor-derived factors. We also found that hemin conditioning limits the tumor angiogenic process *in vivo*. We have previously documented the anti-angiogenic properties of HO-1 induction in the PCa epithelial compartment (15). Moreover, this anti-angiogenic effect was also demonstrated in pancreatic cancer by exogenous administration of the HO-1 metabolic product CO (35). In line with these

observations, Ahmad *et al* (36) recently reported that CO exposure inhibits VEGF-induced endothelial cell proliferation, migration and capillary-like tube formation. Furthermore, in our pre-clinical model we found that Gal-1 expression was significantly reduced in tumors generated in hemin-treated mice. Our previous findings have shown that this lectin is highly expressed and regulated in the PCa microenvironment and plays a major role in PCa neovascularization (23). Notably, Croci *et al* (25,37) elegantly demonstrated the existence of a glycosylation-based circuit in which Gal-1 interaction with VEGFR2 mimics VEGF-A function and induces angiogenesis. Here we confirmed that Gal-1 promotes the formation of tube-like structures *in vitro*. Strikingly, hemin treatment sensitized endothelial cells to apoptosis in a Gal-1-dependent dose (***Figure 2***). It has been previously reported that endothelial cells may undergo Gal-1-induced apoptosis when a potential co-receptor for VEGFR-2, CD146, is down-regulated (29,30); in this regard, we have indeed confirmed that hemin treatment upon endothelial cells inhibits CD146 expression. Moreover, taking into consideration the prolonged inhibition of Gal-1 expression in tumors evidencing impaired growth, our data might indicate that hemin conditioning remodels the endothelial compartment, affecting its interaction with the tumor cell. However, other studies have reported pro-angiogenic roles for HO-1 and its metabolic products in different cancer models and other pathologies (reviewed in 12,38), providing evidence of the inconsistent function of HO-1 in tumorigenesis and unveiling the complexity of the angiogenic process. Thus, the role of this protein is far from clear, but the general consensus of opinion is that its effect is highly dependent on tumor type, the trigger of tissue-specific signaling pathways, and the relative contribution of the enzymatic products and the non-canonical roles.

Nevertheless, simultaneous targeting of multiple components of the tumor microenvironment will be required to achieve a durable and efficient anti-tumor response. Our results indicate that hemin conditioning can also boost the immune response (***Figures 3 and 4***). Hemin treatment resulted in enhanced $CD8^+$ T-cell proliferation and degranulation but, more importantly, we have provided strong evidence that subcutaneous administration of this agent augments *in vivo* antigen-specific cytotoxicity.

Outstandingly, assays encompassing *ex vivo* lymph node hemin treatment prior to adoptive transfer supported hemin capacity to boost the $CD8^+$ cytotoxic function, which might in turn account for T-C1 tumor growth impairment. Indeed, we also observed a significant systemic expansion of $CD8^+$ T cells, suggesting that hemin conditioning may trigger long-term immunological effects. Although the immunomodulatory function of HO-1 is well documented and its immunosuppressive role is widely accepted (31), relatively little attention has been paid to the effect of its substrate heme on the immune response. Remarkably, heme directly regulates various molecular and cellular processes, has been shown to act as a T-cell mitogen *in vitro* (39) and exerts mild pro-inflammatory responses encompassing the activation of macrophages and polymorphonuclear cells (40–42). Furthermore, recent findings have shown that oral administration of heme prior to induction of necrotizing enterocolitis decreased disease incidence and increased Treg/Teff ratios (43). In addition, Konrad and collaborators (44) demonstrated that topical administration of hemin was protective against pulmonary inflammation. Both studies have clearly associated the reported effects to HO-1 expression by using genetically modified animals. Two independent studies have shown that HO-1 expressed in macrophages may influence PCa tumor fate and promote its growth (45,46). Surprisingly, Jais and collaborators (47) claimed to have broken the HO-1 dogma by providing evidence of its pro-inflammatory role in hepatocytes and macrophages in the development of metabolic disease, using conditional genetically-modified mice and patient data sets. In addition, Mashreghi *et al* (48) showed that pharmacological agents usually associated to HO-1 modulation have the capacity to shape the immune response independently of this protein. Thus, we may conclude that under our pre-clinical model hemin could trigger a complex immune response, characterized by augmented $CD8^+$ T-cell function. Finally, Gal-1 downregulation in tumors grown in hemin-conditioned animals might reflect potentiation of a tumor-specific immune response, as several findings indicate that this lectin plays critical pro-tumorigenic roles within the tumor microenvironment, in part by suppressing T cell-mediated cytotoxic responses (reviewed in 32,49). The relevance of the immune system in our experimental model becomes plainly evident when immunodeficient mice were conditioned with hemin prior to tumor

challenge, as no significant differences were found. Although immunodeficient mice provide valuable information in cancer research, our findings add to cumulative data in literature that urge for fully immunocompetent and syngeneic animal models.

Finally, to assess the potential clinical implications of both HO-1 and Gal-1 in PCa, we searched the cancer database Oncomine. Interestingly, a subset of patients displays mild up-regulation of HO-1 with significantly lower expression for Gal-1, when comparing prostate adenocarcinoma vs. normal gland (***Table 1*** and ***Figure S3***). This was further evidenced by the analysis of PDXs, which also showcased a subgroup with mild HO-1 and low Gal-1 expression (***Table 2***). This subpopulation could potentially be more susceptible to hemin treatment as an adjuvant therapy, maintaining Gal-1 expression levels severely low and, in combination with other anti-angiogenic and/or immune therapies, might interrupt tumor growth and/or spread.

To summarize, our work provides evidence of the effect of hemin conditioning in both vascular and immune compartments, and its implications on PCa development. Our strategy was conceived to remodel the environment to counteract the effects of tumor-escape mechanisms. We speculate that novel therapeutic interventions should be designed to specifically target the reactive stroma. As mentioned above, we have previously shown that hemin treatment in prostate cancer cell lines does not have toxic effects and it even impairs proliferation, migration and invasion *in vitro* and HO-1 over-expression leads to smaller and less vascularized tumors *in vivo* (14,15). It should be noted that there is a considerable number of reports showcasing the pro-tumor role of HO-1 in different types of cancer, even in PCa (20,21). Consequently, further study should be carried out to elucidate the HO-1 function in cancer development. We are currently developing new experimental strategies to assess hemin effects on prostate tumor progression *in vivo*, including intratumor injections and other means of specifically targeting immune and endothelial cells infiltrating the tumor. The results from this paper provide a solid proof of concept to move forwards in this direction.

Acknowledgments

We are grateful to PCF (USA) for the Young Investigator Award 2013 given to GG, and to EMBO for the Short-term fellowship awarded to FMJ.

References

1. Ferlay J, Soerjomataram I, Ervik M, Dikshit R, Eser S, Mathers C, et al. GLOBOCAN 2012 v1.0, Cancer Incidence and Mortality Worldwide: IARC CancerBase. No. 11 [Internet]. Lyon, France: International Agency for Research on Cancer. Published 2013.

2. Quail DF, Joyce JA. Microenvironmental regulation of tumor progression and metastasis. Nat Med. 2013;19:1423-1437.

3. Corn PG. The tumor microenvironment in prostate cancer: Elucidating molecular pathways for therapy development. Cancer Manag Res. 2012;4:183-193.

4. Hanna E, Quick J, Libutti SK. The tumour microenvironment: A novel target for cancer therapy. Oral Dis. 2009;15:8-17.

5. Grivennikov SI, Greten FR, Karin M. Immunity, Inflammation, and Cancer. Cell. 2010;140:883-899.

6. Mantovani A, Allavena P, Sica A, Balkwill F. Cancer-related inflammation. Nature. 2008;454:436-444.

7. Hanahan D, Weinberg R a. Hallmarks of cancer: the next generation. Cell. 2011;144:646-674.

8. Jackson JR, Seed MP, Kircher CH, Willoughby DA, Winkler JD. The codependence of angiogenesis and chronic inflammation. FASEB J. 1997;11:457-465.

9. Mantovani A. Molecular pathways linking inflammation and cancer. Curr Mol Med. 2010;10:369-373.

10. Gozzelino R, Jeney V, Soares MP. Mechanisms of cell protection by heme oxygenase-1. Annu Rev Pharmacol Toxicol. 2010;50:323-354.

11. Wegiel B, Nemeth Z, Correa-Costa M, Bulmer AC, Otterbein LE. Heme oxygenase-1: a metabolic nike. Antioxid Redox Signal. 2014;20:1709-1722.

12. Was H, Dulak J, Jozkowicz A. Heme oxygenase-1 in tumor biology and therapy. Curr Drug Targets. 2010;11:1551-1570.

13. Grochot-Przeczek A, Dulak J, Jozkowicz A. Haem oxygenase-1: non-canonical roles in physiology and pathology. Clin Sci (Lond). 2012;122:93-103.

14. Gueron G, De Siervi A, Ferrando M, Salierno M, De Luca P, Elguero B, et al. Critical role of endogenous heme oxygenase 1 as a tuner of the invasive potential of prostate cancer cells. Mol Cancer Res. 2009;7:1745-1755.

15. Ferrando M, Gueron G, Elguero B, Giudice J, Salles a, Leskow FC, et al. Heme oxygenase 1 (HO-1) challenges the angiogenic switch in prostate cancer. Angiogenesis. 2011;14:467-479.

16. Ferrando M, Wan X, Meiss R, Yang J, De Siervi A, Navone N, et al. Heme oxygenase-1 (HO-1) expression in prostate cancer cells modulates the oxidative response in bone cells. PLoS One. 2013;8:e80315.

17. Gueron G, Giudice J, Valacco P, Paez A, Elguero B, Toscani M, et al. Heme-oxygenase-1 implications in cell morphology and the adhesive behavior of prostate cancer cells. Oncotarget. 2014;5:4087-4102.

18. Paez A, Pallavicini C, Schuster F, Valacco MP, Giudice J, Ortiz EG, et al. Heme Oxygenase-1 at the forefront of a multi-molecular network that governs cell-cell contact and filopodia-induced zippering in prostate cancer. Cell Death and Disease. 2016; 7:e2570.

19. Elguero B, Gueron G, Giudice J, Toscani MA, De Luca P, Zalazar F, et al. Unveiling the association of STAT3 and HO-1 in prostate cancer: role beyond heme degradation. Neoplasia. 2012;14:1043-1056.

20. Alaoui-jamali MA, Bismar TA, Gupta A, Szarek WA, Su J, Song W, et al. A novel experimental heme oxygenase-1-targeted therapy for hormone-refractory prostate cancer. Cancer Res. 2009;69:8017-8024.

21. Li Y, Su J, DingZhang X, Zhang J, Yoshimoto M, Liu S, et al. PTEN deletion and heme oxygenase-1 overexpression cooperate in prostate cancer progression and are associated with adverse clinical outcome. J Pathol. 2011;224:90-100.

22. Wegiel B, Gallo D, Csizmadia E, Harris C, Belcher J, Vercellotti GM, et al. Carbon monoxide expedites metabolic exhaustion to inhibit tumor growth. Cancer Res. 2013;73:7009-7021.

23. Laderach DJ, Gentilini LD, Giribaldi L, Delgado VC, Nugnes L, Croci DO, et al. A unique galectin signature in human prostate cancer progression suggests galectin-1 as a key target for treatment of advanced disease. Cancer Res. 2013;73:86-96.

24. Li ZG, Mathew P, Yang J, Starbuck MW, Zurita AJ, Liu J, et al. Androgen receptor – negative human prostate cancer cells induce osteogenesis in mice through FGF9-mediated mechanisms. J. Clin. Invest. 2008;118:2697-2710.

25. Croci DO, Cerliani JP, Dalotto-Moreno T, Méndez-Huergo SP, Mascanfroni ID, Dergan-Dylon S, et al. Glycosylation-dependent lectin-receptor interactions preserve angiogenesis in anti-VEGF refractory tumors. Cell. 2014;156:744-758.

26. Rhodes DR, Yu J, Shanker K, Deshpande N, Varambally R, Ghosh D, et al. ONCOMINE: A Cancer Microarray Database and Integrated Data-Mining Platform1. Neoplasia. 2004;6:1-6.

27. Gentilini LD, Jaworski FM, Tiraboschi C, Gonzalez Perez I, Kotler M, Chauchereau A, Laderach D et al. Stable and high expression of Galectin-8 tightly controls metastatic progression of prostate cancer. Oncotarget (in press).

28. Ellerhorst J, Troncoso P, Xu XC, Lee J, Lotan R. Galectin-1 and galectin-3 expression in human prostate tissue and prostate cancer. Urol Res. 1999;27:362-367.

29. Jouve N, Despoix N, Espeli M, Gauthier L, Cypowyj S, Fallague K, et al. The Involvement of CD146 and Its Novel Ligand Galectin-1 in Apoptotic Regulation of Endothelial Cells. J Biol Chem. 2013;288:2571-2579.

30. Jiang T, Zhuang J, Duan H, Luo Y, Zeng Q, Fan K, et al. CD146 is a coreceptor for VEGFR-2 in tumor angiogenesis. Blood. 2012;120:2330-2339.

31. Blancou P, Tardif V, Simon T, Rémy S, Carreño L, Kalergis A, et al. Immunoregulatory properties of Heme Oxygenase-1. Methods Mol Biol. 2011;677:431-447.

32. Rabinovich GA, Croci DO. Regulatory Circuits Mediated by Lectin-Glycan Interactions in Autoimmunity and Cancer. Immunity. 2012;36:322-335.

33. Grasso CS, Wu Y-M, Robinson DR, Cao X, Dhanasekaran SM, Khan AP, et al. The mutational landscape of lethal castration-resistant prostate cancer. Nature. 2012;487:239-243.

34. Bouma-Ter Steege JCA, Baeten CIM, Thijssen VLJL, Satijn SA, Verhoeven ICL, Hillen HFP, et al. Angiogenic profile of breast carcinoma determines leukocyte infiltration. Clin Cancer Res. 2004;10:7171-7178.

35. Vítek L, Gbelcová H, Muchová L, Váňová K, Zelenka J, Koníčková R, et al. Antiproliferative effects of carbon monoxide on pancreatic cancer. Dig Liver Dis. 2014;46:369-375.

36. Ahmad S, Hewett PW, Fujisawa T, Sissaoui S, Cai M, Gueron G, et al. Carbon monoxide inhibits sprouting angiogenesis and vascular endothelial growth factor receptor-2 phosphorylation. Thromb Haemost. 2015;113:329-337.

37. Croci DO, Salatino M, Rubinstein N, Cerliani JP, Cavallin LE, Leung HJ, et al. Disrupting galectin-1 interactions with N-glycans suppresses hypoxia-driven angiogenesis and tumorigenesis in Kaposi's sarcoma. J Exp Med. 2012;209:1985-2000.

38. Szade A, Grochot-Przeczek A, Florczyk U, Jozkowicz A, Dulak J. Cellular and molecular mechanisms of inflammation-induced angiogenesis. IUBMB Life. 2015;67:145-159.

39. Stenzel K, Rubin A, Novogrodsky A. Mitogenic and co-mitogenic properties of hemin. J Immunol. 1981;127:2469-2473.

40. Graça-Souza AV, Arruda MAB, De Freitas MS, Barja-Fidalgo C, Oliveira PL. Neutrophil activation by heme: Implications for inflammatory processes. Blood. 2002;99:4160-4165.

41. Figueiredo RT, Fernandez PL, Mourao-Sa DS, Porto BN, Dutra FF, Alves LS, et al. Characterization of heme as activator of toll-like receptor 4. J Biol Chem. 2007;282:20221-20229.

42. Porto BN, Alves LS, Fernández PL, Dutra TP, Figueiredo RT, Graça-Souza AV, et al. Heme induces neutrophil migration and reactive oxygen species generation through signaling pathways characteristic of chemotactic receptors. J Biol Chem. 2007;282:24430-24436.

43. Schulz S, Chisholm K, Zhao H, Kalish F, Yang Y, Wong R, et al. Heme oxygenase-1 confers protection and alters T-cell populations in a mouse model of neonatal intestinal inflammation. Pediatr Res. 2015;640-648.

44. Konrad F, Knausberg U, Hone R, Ngamsri K-C, Reutershan J. Tissue heme oxygenase-1 exerts anti-inflammatory effects on LPS-induced pulmonary inflammation. Mucosal Immunol. 2016;99-111.

45. Nemeth Z, Li M, Csizmadia E, Döme B, Johansson M, Person J, et al. Heme oxygenase-1 in macrophages controls prostate cancer progression. Oncotarget. 2015;6:33675-33688.

46. Halin Bergstrom S, Halin Bergstrom S, Nilsson, M, Adamo H, Thysell E, Jernberg E, Stattin P, et al. Extratumoral Heme Oxygenase-1 (HO-1) Expressing Macrophages Likely Promote Primary and Metastatic Prostate Tumor Growth. PLoS One. 2016;11,e0157280.

47. Jais A, Einwallner E, Sharif O, Gossens K, Lu TTH, Soyal SM, et al. Heme oxygenase-1 drives metaflammation and insulin resistance in mouse and man. Cell. 2014;158:25-39.

48. Mashreghi M-F, Klemz R, Knosalla IS, Gerstmayer B, Janssen U, Buelow R, et al. Inhibition of dendritic cell maturation and function is independent of heme oxygenase 1 but requires the activation of STAT3. J Immunol. 2008;180:7919-7930.

49. Rabinovich GA, Toscano MA. Turning “sweet” on immunity: galectin-glycan interactions in immune tolerance and inflammation. Nat Rev Immunol. 2009;9:338-352.

	HMOX1	*LGALS1*	*CD34*	*FLT1*	*FLT4*	*KDR*	*VEGFA*	*VEGFC*	*VCAM1*	*CD28*	*CD80*	*CD86*
Grasso *et al*	1.295 0.033 Top 25%	-1.708 7.23E-06 Top 7	-1.179 0.045 Top 31%	-1.999 0.01 Top 23%	-1.214 0.007 Top 22%		-1.656 0.008 Top 22%	-1.431 4.18E-06 Top 7%	1.267 0.034 Top 25%	1.373 0.036 Top 26%	1.428 0.004 Top 15%	4.127 9.52E-04 Top 12%
Varambally *et al*	2.292 0.002 Top 3%	-1.511 0.03 Top 19%		-1.731 0.01 Top 11%			-1.975 0.009 Top 11%	-1.254 0.043 Top 22%		2.245 0.003 Top 4%	1.21 0.244 Top 40%	2.442 0.0071 Top 19%
Taylor *et al*	1.078 0.019 Top 19%	-1.548 0.019 Top 2%	-1.093 0.022 Top 19%			-1.127 0.042 Top 21%	-1.272 0.007 Top 15%		1.232 0.002 Top 9%	1.109 4.31E-04 Top 4%	1.144 3.19E-04 top 6%	1.138 1.26E-04 Top 5%
Lapointe *et al*	1.188 2.65E-04 Top 13%		-1.249 0.005 Top 21%	-1.432 4.19E-04 Top 16%			-1.55 3.26E-06 Top 9%			1.009 0.46 Top 58%	1.035 0.298 Top 52%	1.041 0.292 Top 52%

Table 1. Summary table of results obtained for each database using Oncomine. Table depicts gene name, fold-induction (adenocarcinoma vs. normal gland), *P*-value and gene rank. Lower panel shows a heat map indicating the level of expression for each gene in each study (blue: under-expressed, red: over-expressed).

PDX		HO-1 expression	Gal-1 expression	Histopathology of human tumor of origin	Tumor site
MDA PCa 144 (three PDXs from diferent areas of the same tumor)	*MDA PCa 144-13*	0.5 to 1.0	0.0	Mixed Adenocarcinoma and Small Cell Carcinoma with Neuroendocrine Differentiation	Local extension of prostate cancer to bladder
	MDA PCa 144-23	1.5	0.0	Mixed Adenocarcinoma and Small Cell Carcinoma with Neuroendocrine Differentiation	Local extension of prostate cancer to rectal wall
	MDA PCa 144-20	1.5	0.2	Mixed Adenocarcinoma and Small Cell Carcinoma with Neuroendocrine Differentiation	Local extension of prostate cancer to rectal wall
MDA PCa 155 (two PDXs from diferent areas of the same tumor)	*MDA PCa 155-2*	1.5	0.3	Poorly diferentiated carcinoma with Neuroendocrine features	Local extension of prostate cancer to bladder neck
	MDA PCa 155-12	1.0	0.5	Poorly diferentiated carcinoma with Neuroendocrine features	Local extension of prostate cancer to bladder neck
	MDA PCa 160-29	0.9	0.6	prostatic sarcomatoid adenocarcinoma	Local extension of prostate cancer to intraprostatic urethra
MDA PCa 150 (two PDXs from diferent areas of the same tumor) (*)	*MDA PCa 150-5*	1.0	0.7	Poorly diferentiated carcinoma with Neuroendocrine features	Bone
	MDA PCa 150-3	1.5	0.8	Poorly diferentiated carcinoma with Neuroendocrine features	Bone
	MDA PCa 178-11	0.5 to 1.0	1.0	Adenocarcinoma	Prostate
	MDA PCa 182-7	1.0	1.3	Adenocarcinoma	Prostate
MDA PCa 150 (*)	*MDA PCa 150-7*	0.9 to 1.0	2.0	Poorly diferentiated carcinoma with Neuroendocrine features	Bone
	MDA PCa 166-1	1.3	2.0	Adenocarcinoma	Local extension of prostate cancer to bladder neck
MDA PCa 153 (two PDXs from diferent areas of the same tumor)	*MDA PCa 153-14*	1.0 to 1.8	2.1	Adenocarcinoma with Neuroendocrine Differentiation	Thyroid
	MDA PCa 153-7	0.5 to 1.0	2.33 to 2.5	Adenocarcinoma with Neuroendocrine Differentiation	Thyroid
	MDA PCa 188-2	0.5	2.2	Adenocarcinoma	Local extension of prostate cancer to bladder
	MDA PCa 118b	0.7	3.0	adenocarcinoma	Bone
	MDA PCa 180	1.5	3.0	Adenocarcinoma	Local extension of prostate cancer to bladder

Table 2. Tissue microarray data corresponding to PDXs with low-to-intermediate staining for HO-1. The table summarizes Gal-1 expression score, pathology diagnosis, anatomical description and tumor site, for each of the PDXs. Semi-quantitative studies were carried out by a pathologist (RPM); IHC staining was scored as follows: 0, no staining; 1, low staining; 2, mild staining; 3, high staining. PDXs are ordered vertically from top to bottom according to increasing Gal-1 expression.

Legends to figures

Figure 1. Hemin conditioning blunts PCa tumor development. C57BL/6 mice (n=5) were subcutaneously injected with hemin (200µl, 30µM) on days -8, -5 and -1 prior to tumor challenge on the same flank ($2x10^6$ T-C1 cells in Matrigel). Control littermates were injected with PBS. In all cases, empty circles represent control mice and filled circles depict hemin-conditioned mice. **A,** schematic representation of the experimental protocol. **B,** tumor growth follow-up. Left panel depicts the percentage of tumor-free mice along the course of the experiment. Solid line, control animals; dashed line, hemin pre-treated mice. ** indicates $P<0.01$, Mantel-Cox test. Normalized tumor volume evolution is shown in the right panel. * indicates $P<0.05$ when comparing data contained in the shadowed box; Student *t* test. **C,** histological analysis of paraffin-embedded tumor sections obtained from control or hemin pre-treated mice at the experimental end point. Masson's trichrome staining and CD31 immunohistochemical analysis were performed. Original magnification, x400. **D,** transcriptional analysis of several angiogenesis-related genes. RT-qPCR was performed from tumor total RNA and the relative expression of the following genes was assessed: Vascular Endothelial Growth Factor-A *(Vegfa*), Thrombosplastin (*F3*), Plasminogen Activator, Urokinase (*Plau*), Fibroblast Growth Factor-2 (*Fgf2*), TIMP Metallopeptidase Inhibitor-I (*Timp1*), Thrombospondin (*Thbs1*) and Galectin-1 (*Lgals1*). The murine acidic ribosomal protein P0 gene *Rplp0* was used as an internal reference gene. ** indicates $P<0.01$, Student *t* test.

Figure 2. Hemin remodels the interaction between the endothelial cell and the prostate tumor cell. A, expression of *HMOX1* mRNA levels in control and hemin-treated HUVEC (50µM, 8h), as determined by RT-qPCR 16h after hemin treatment. Human cyclophilin A gene *PPIA* was used as an internal reference gene. *** indicates $P<0.001$; n=3; Student *t* test. **B,** *in vitro* tube formation using control or hemin-treated HUVEC in the absence or presence of T-C1 conditioned media. Binary tree-structures were obtained from original microscopic photographs. Complete growth media served as a positive control. Figure depicts one representative out of three independent experiments. **C,** total tube

length was quantified. *** indicates *P*<0.001; n=3; Two-way ANOVA. **D,** Gal-1-induced apoptosis was assessed on both control and hemin pre-treated endothelial cells, by measuring Annexin-V (An-V) binding and propidium iodine (PI) staining followed by flow cytometry. The left panel depicts representative photographs for the different experimental conditions (original magnification x100). The central panel shows representative dot plots obtained by flow cytometry for the different experimental conditions. The right panel shows the quantification of viable and early apoptotic cells. * indicates *P*<0.05; ** indicates *P*<0.01; and *** indicated *P*<0.001; n=4; Two-way ANOVA. **E,** the effect of control or hemin-treated HUVEC conditioned-media on TC-1 migration was evaluated through a wound-scratch assay. Photographs taken 48h after scratch show representative images. Wound area was quantified 12, 24 and 48h after scratch (right panel). * indicates *P*<0.05; *** indicates *P*<0.001; n=3; Student *t* test. **F,** T-C1 adhesion to hemin pre-treated HUVEC was assessed by adding CFSE-labeled T-C1 cells to an endothelial monolayer. After 2h of incubation at 37°C, detached cells were washed out with PBS and adhered cells were counted under an inverted fluorescent microscope. Photographs show representative images. The right panel shows the number of labeled T-C1 cells per field. ** indicates *P*<0.01; n=3; Student *t* test. **G**, T-C1 cells in Matrigel were subcutaneously injected into C57BL/6 mice following hemin conditioning (n=5). Five days later, Matrigel plugs were harvested and photographed. The right panel shows representative plugs. Once homogenized, hemoglobin and total protein content were determined. The left panel depicts hemoglobin content relative to total protein content. * indicates *P*<0.05, Student *t* test. In all cases, empty circles represent control conditions and filled circles depict hemin treatments. **H,** samples of blood vessel-containing tissue derived from the injected flank were retrieved on the day that mice would have been challenged with tumor cells, and CD31 and HO-1 expression levels were assessed by flow cytometry. Left panel shows a representative histogram per experimental condition. Right panel depicts the mean fluorescence intensity for each mouse; * indicates *P*<0.05; Student *t* test.

Figure 3. Hemin enhances CD8$^+$ CTL responses. A-E, results depict one representative out of three independent experiments. **A,** lymph node cells were cultured with hemin (8h; 18.75, 37.5 and 75μM) and HO-1 expression assessed by intracytoplasmatic staining; numbers indicate mean fluorescence intensity. **B,** CD8$^+$ T-cell proliferation in response to coated anti-CD3 antibody (1 μg/ml). T-C1 cells were added to mimic a tumor microenvironment. Cultures were treated with hemin (18.75, 37.5 and 75μM). CFSE dilution was assessed 72h post-stimulation. **C,** CD8$^+$ T-cell degranulation in response to coated anti-CD3 antibody (1μg/ml) was measured by CD107a mobilization to the plasma membrane. Cells were stimulated in the presence or absence of hemin (12h; 75μM) and stained for extracellular CD107a. **D-E,** lymph node cells were co-cultured with T-C1 cells for 24h in an anti-CD3-coated well (1μg/ml). Hemin (18.75, 37.5 and 75μM) was then added and proliferation was measured after 72h as previously described. Alternatively, degranulation was measured after 12h as previously described. **F-H,** *in vivo* CD8$^+$ cytotoxicity assays. Empty circles represent control mice; filled circles depict hemin-conditioned mice. **F,** schematic representation of the *in vivo* OVA-specific cytotoxicity assay. **G,** expression of *HMOX1* mRNA levels in inguinal, brachial and axillary lymph nodes retrieved from both hemin-treated and control animals, as determined by RT-qPCR. Samples were collected on the day following the last subcutaneous injection. * indicates $P<0.05$; Student *t* test. **H,** OT-1 lymph node cell-transferred mice (n=5) were treated with hemin and subsequently challenged with a mix of $CFSE_{dim\text{-}OVA}$ and $CFSE_{bright\text{-}ctrl}$ cells (1:1). After 16h, their relative proportion was evaluated by flow cytometry of splenic homogenates (left panel). The right panel shows the percentage of OVA-specific cytotoxicity. ** indicates $P<0.01$, Student *t* test. **I,** hemin treatment was performed *ex vivo* (8h; 75μM) prior to adoptive transfer into non-irradiated C57BL/6 mice (n=5). Animals were subsequently challenged with $CFSE_{dim\text{-}OVA}$ and $CFSE_{bright\text{-}ctrl}$ cells and 16h later sacrificed for cytotoxicity analysis. The figure shows the percentage of OVA-specific cytotoxicity. ** indicates $P<0.01$, Student *t* test.

Figure 4. Hemin conditioning shapes immunological and vascular compartments and restrains prostate tumor growth. A-D, T-C1 tumor-bearing mice (n=4) were sacrificed when control mice

exhibited tumors in their exponential growth phase while hemin pre-treated mice showed tumors in their initial growth steps. In all cases, empty circles represent control mice and filled circles depict hemin-conditioned mice. **A,** tumor, spleen and tumor-draining lymph node (TDLN) samples were evaluated for $CD8^+$ T cell frequency using flow cytometry. * indicates $P<0.05$; ** indicates $P<0.01$, Student *t* test. **B,** TDLN samples were assessed for $CD11b^+Gr\text{-}1^+$ cell frequency using flow cytometry. * indicates $P<0.05$; Student *t* test. **C,** histological analysis of paraffin-embedded tumor sections obtained from control or hemin pre-treated mice. Masson's trichrome staining and CD31 immunohistochemical analysis were performed. Upper panel, original magnification, x100. Central and lower panels, original magnification, x400; arrows depict atypical mitotic figures. **D,** immunohistochemical staining against Gal-1 performed on paraffin-embedded tumor sections obtained from control or hemin pre-treated mice. IgG refers to the control staining with rabbit pre-immune sera. Original magnification, x400. **E,** C57BL/6 mice challenged with T-C1 on the right flank were previously conditioned with hemin either on the same or the opposite flank (ipsilateral, n=10; and contralateral flank, n=5; respectively). Control littermates were injected with PBS on the same flank (n=8). Figure shows the percentage of tumor-free mice along the course of the experiment. Solid line, control condition; black dashed line, hemin conditioning on the ipsilateral flank; grey dashed line, hemin conditioning on the contralateral flank. *** indicates $P<0.001$, Mantel-Cox test. **F,** athymic nude mice (n=5) were subcutaneously injected with hemin prior to tumor challenge on the same flank. Control littermates were injected with PBS. Normalized tumor volume evolution is shown; empty circles represent control mice and filled circles depict hemin pre-conditioned mice.

Author Manuscript Published OnlineFirst on May 16, 2017; DOI: 10.1158/1078-0432.CCR-17-0112
Author manuscripts have been peer reviewed and accepted for publication but have not yet been edited.

Figure 1

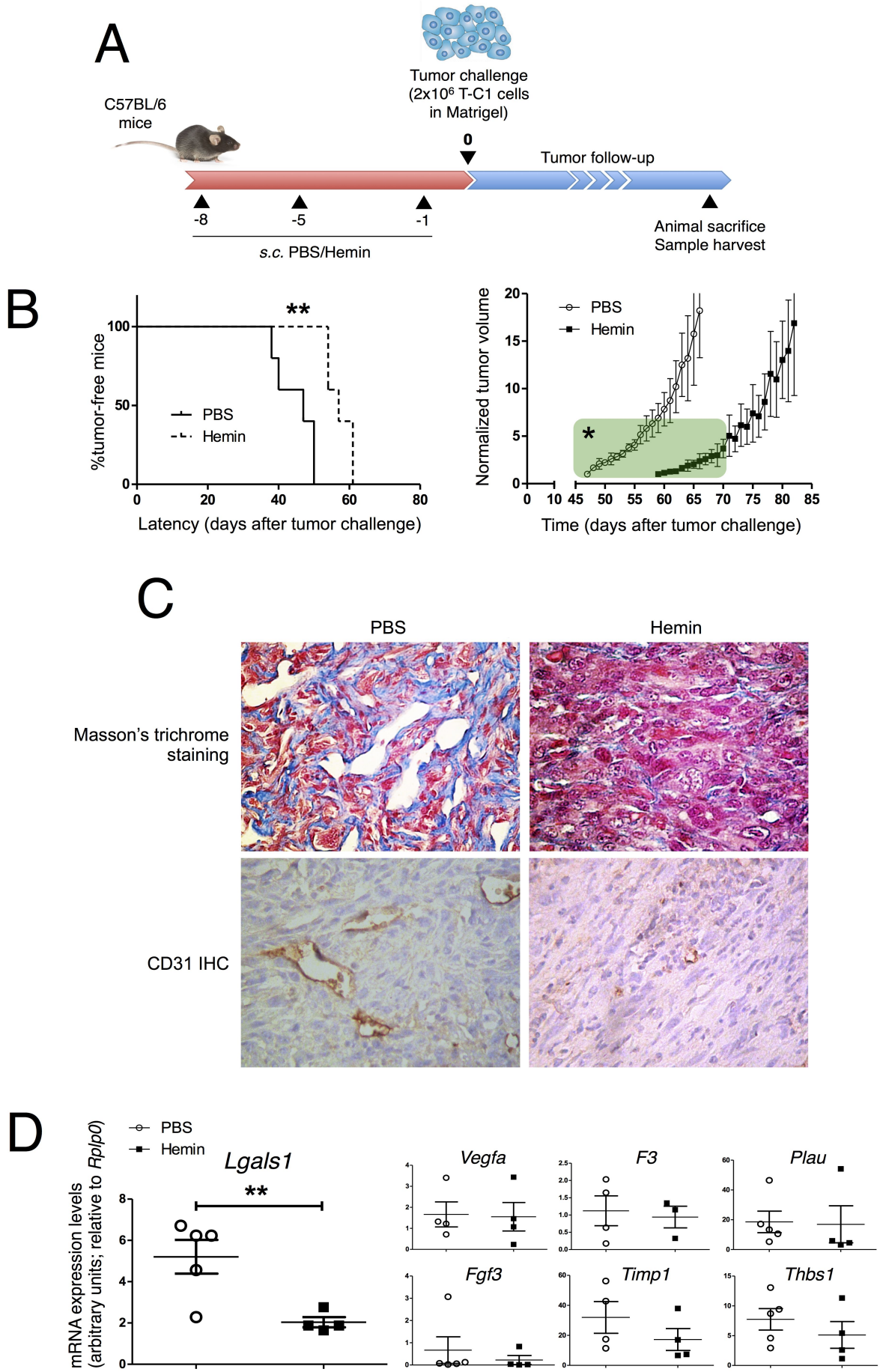

Figure 2

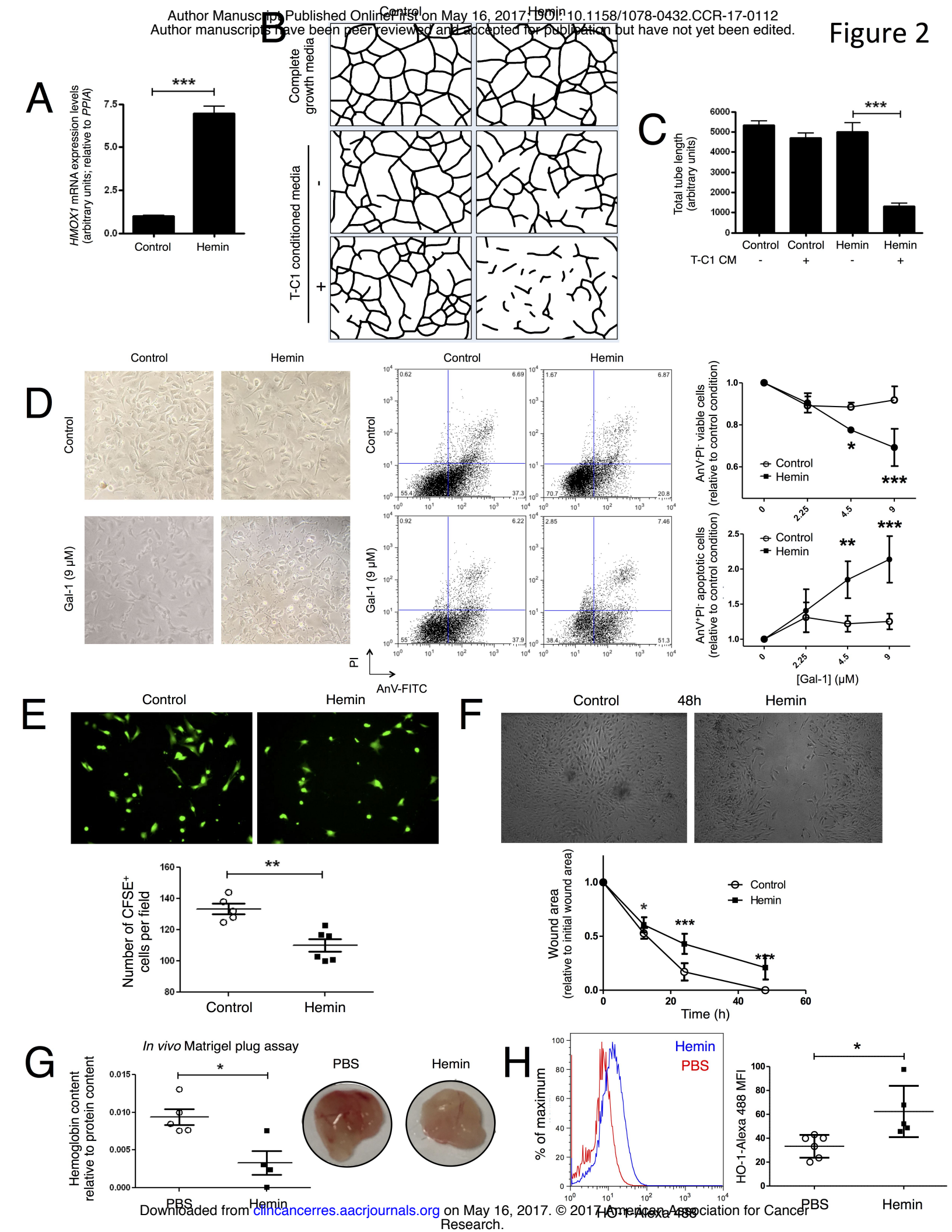

Author Manuscript Published OnlineFirst on May 16, 2017; DOI: 10.1158/1078-0432.CCR-17-0112
Author manuscripts have been peer reviewed and accepted for publication but have not yet been edited.

Figure 3

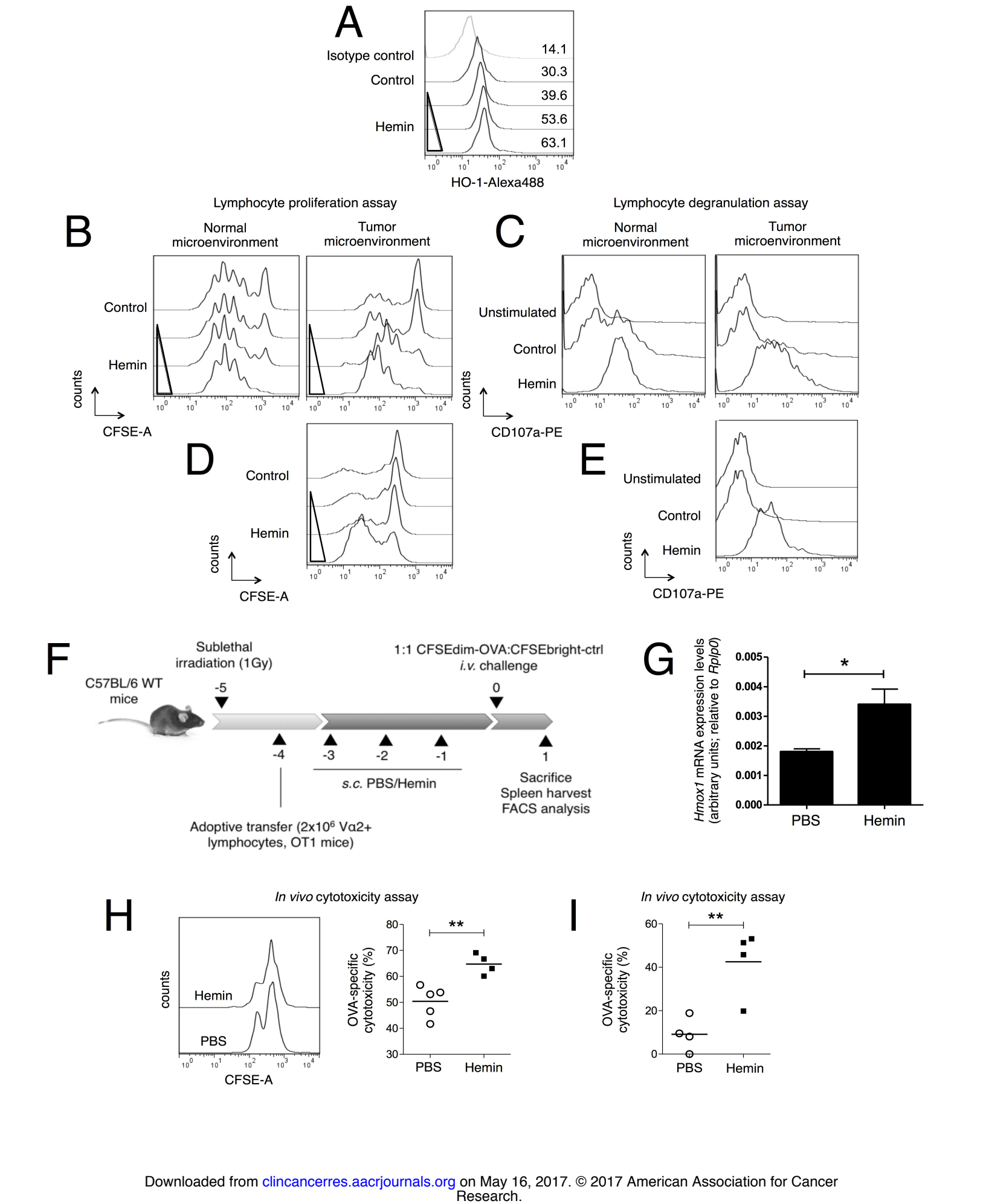

Author Manuscript Published OnlineFirst on May 16, 2017; DOI: 10.1158/1078-0432.CCR-17-0112
Author manuscripts have been peer reviewed and accepted for publication but have not yet been edited.

Figure 4

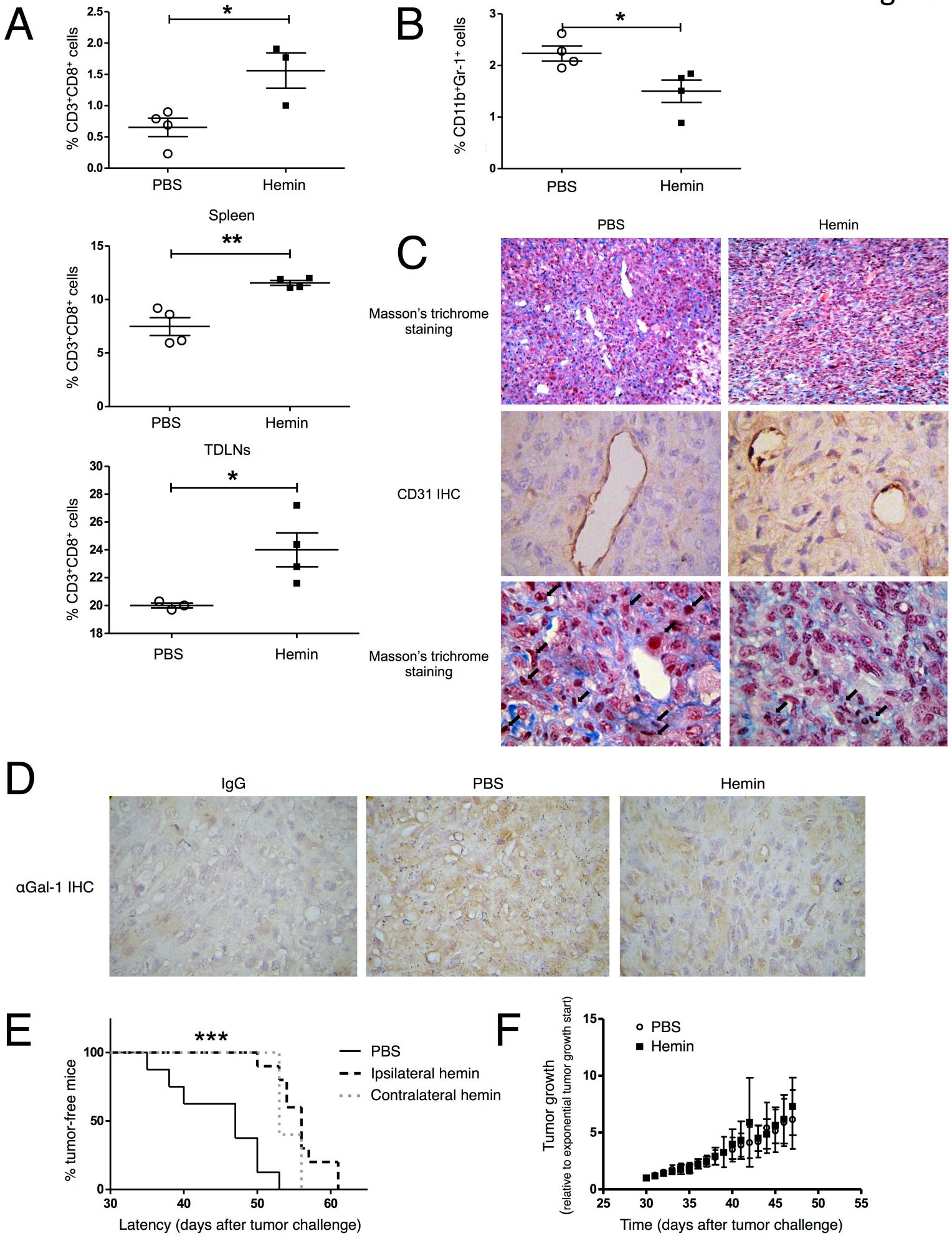

AACR American Association for Cancer Research

Clinical Cancer Research

In vivo hemin conditioning targets the vascular and immunological compartments and restrains prostate tumor development

Felipe M Jaworski, Lucas Gentilini, Geraldine Gueron, et al.

Clin Cancer Res Published OnlineFirst May 16, 2017.